Chin. J. Astron. Astrophys. Vol. 6 (2006), No. 1, 61–68
(*http://www.chjaa.org*)

Chinese Journal of
Astronomy and
Astrophysics

A Study of the Molecular Cloud S64 with Multiple Lines of CO Isotopes *

Lei Zhu, Yue-Fang Wu and Yue Wei

Department of Astronomy, Peking University, Beijing 100871; *yfwu@vega.pku.edu.cn*

Received 2005 April 13; accepted 2005 November 17

Abstract We report on a study of the molecular cloud S64 with observations at millimeter wavelengths of multiple molecular lines of CO isotopes. A weak outflow is found, and its physical parameters are estimated. The departure of the core of S64 from the S64 HII region indicates that there are still other star formation activities in that region.

Key words: stars: formation — ISM: clouds — ISM: individual: S64 — ISM: jets and outflows — ISM: evolution — ISM: kinematics and dynamics

1 INTRODUCTION

One of the most exciting fields in the frontier of astrophysics now is the formation of massive stars. However, due to the serious light extinction by gases and dust, it is very difficult to unveil the nature of early massive stellar objects and their environment. HII regions are produced by massive stars, and play an important role in the process of massive star formation. The natal massive stars are deeply embedded in molecular clouds, and the high energy radiation from them will ionize the surrounding matter and produce HII regions, which look like some expanding ionized cavities. Wood & Churchwell (1989) gave a classification of the ultra-compact (UC) HII regions. A blister model for UC HII regions has been advanced and discussed by several authors (e.g., York et al. 1983). As important tracers of massive star formation regions, HII regions are usually bright in infrared wavelengths, for the reason that the dusty surroundings absorb optical and ultraviolet radiation of the newly formed stars and reradiate them in longer wavelengths (Goldreich & Kwan 1974). The study of HII regions is a key point which can further our understanding of new massive stars in formation and their birthplaces. Besides the sources which ionize the HII regions, many star formation phenomena are found in the ambient environment, such as outflows (Wu et al. 2004), water masers (Esimbek et al. 2005) and HH objects (Wu et al. 2002).

S64 (Sharpless 1959), also known as W40 (Westerhout et al. 1958), located at $\alpha = 18^{\rm h}28^{\rm m}49^{\rm s}$, $\delta = -02^\circ07'36''$, equinox=1950.0 (Vallée 1987), is a well-studied HII region. It is in a late phase of evolution and shows optical lines. There is a molecular cloud bordering the HII region. Zeilik & Lada (1978) and Crutcher & Chu (1982) suggested that the HII region grew out from the molecular cloud. Vallée (1987) and Vallée et al. (1991, 1992, 1994) studied the physical structure of S64 with the carbon recombination line emission, the free-free continuum emission and CO isotopic lines from the HII region or the molecular cloud. However, these researches focus on the S64 HII region itself and on the relationship between the HII region and the molecular cloud. The accurate structure of the S64 molecular cloud and the question whether star formation is still going on in it are unknown, and no outflow was identified because of the low sensitivity and the region being not

* Supported by the National Natural Science Foundation of China.

full. To answer these questions, we observed S64 in the ^{12}CO J=1–0, 3–2 and ^{13}CO J=2–1, 3–2 transitions. With these multiple lines, the morphologies and physics of the core of the molecular cloud and star formation activities were investigated, and an outflow was identified for the first time. Meanwhile, by comparing our millimeter data and the infrared data of Midcourse Space Experiment (MSX) and IRAS, we understood more about the structure of S64.

Section 2 presents our observations of S64 at millimeter wavelengths, and the results of observations are detailed in Section 3. Section 4 presents a discussion and our conclusions.

2 OBSERVATIONS

^{13}CO J=2–1, 3–2 and ^{12}CO J=3–2 maps were constructed with the KOSMA 3-m telescope of Gornergrat Observatory in Swiss Alps, in 1999 September. All the maps were centered at $\alpha(1950) = 18^{\rm h}28^{\rm m}40.0^{\rm s}$, $\delta(1950) = -02^\circ09'00''$. The beam size of the telescope is 120 arcsec at 230 GHz and 80 arcsec at 345 GHz. Superconductor Insulator Superconductor (SIS) receivers were operated with a double sideband mode, with system temperatures of about 260 K and 330 K for the 230 GHz and 345 GHz bands, respectively. The pointing accuracy was better than 10 arcsec. For 230 GHz, the Acoustic-Optical Spectrograph (AOS) had 1501 channels, a total band of 260 MHz and an equivalent velocity resolution of 0.23 km s^{-1}. For 345 GHz, the corresponding figures are 701 channels, 475 MHz and 0.59 km s^{-1}. The main beam efficiency was 0.67 and the forward efficiency was 0.90.

The ^{12}CO J=1–0 lines were observed with the 13.7-m telescope of Purple Mountain Observatory at the Qinghai Station on 2004 November 16. The beam size is 50 arcsec for the observed wavelength band. An SIS receiver and a new system which can observe the three lines simultaneously were used. The noise temperature of the system, including the atmosphere at zenith, was 250 K. The AOS has a total bandwidths of 145.4 MHz and 1024 channels. The spectral resolution was 209.0 kHz. The pointing accuracy was better than 10 arcsec, and the main beam efficiency was 0.42. All the data reductions were done by CLASS and GREG of GILDAS software.

3 RESULTS

3.1 Outflow

3.1.1 Identification of Outflow

The ^{12}CO lines were used for studying the outflow. Figure 1 shows the ^{12}CO J=1–0 spectrum of S64 at offset position (0, 0), and it seems to include another component at $V_{\rm LSR}$ = 9 km s^{-1}, which is an additional background emission since the spectra at other positions show the same feature. For the ^{12}CO J=3–2 emission the additional component is reduced. Thus in the study of S64 outflow we mainly used the ^{12}CO J=3–2 spectra of KOSMA as the basis for our calculation.

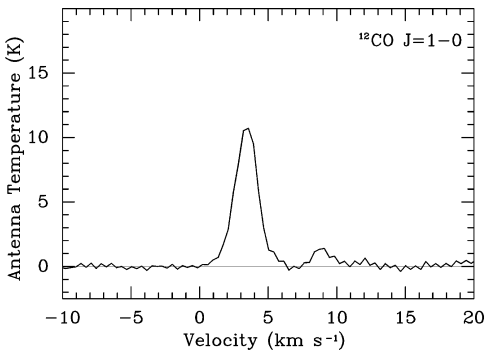

Fig. 1 ^{12}CO J=1–0 spectrum of the (0, 0) point.

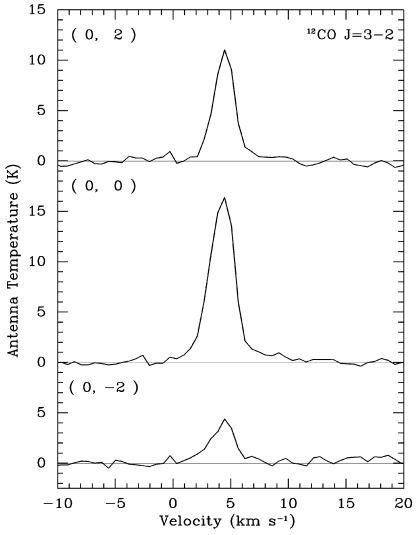

Fig. 2 Three examples of the ^{12}CO J=3–2 lines of S64. The positions are indicated by the offsets, e.g., "(0, 2)" is the offset $\Delta\delta$=0′, $\Delta\alpha$=2′ from the origin at $18^{\rm h}28^{\rm m}40.0^{\rm s}$, $-02^\circ09'00''$ (B1950.0).

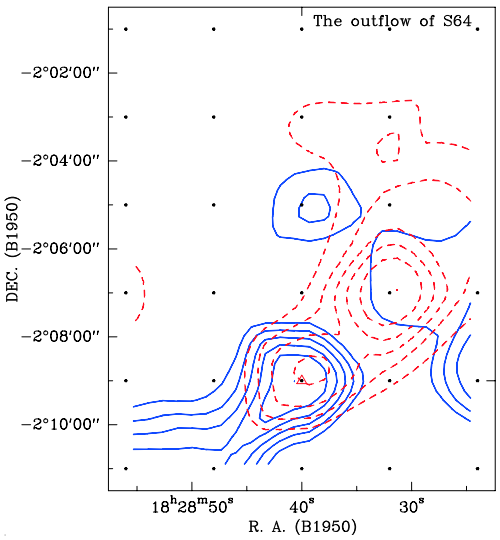

Fig. 3 Integrated contour map of the outflow. The red dashed and blue solid lines indicate the contours of red and blue lobe respectively. The contour levels are from 50%–90% at intervals of 10% for the two lobes, and it should be noted that the maximal integrated intensities of the two are not equal. The triangle indicates the observational origin which is just the center of the outflow.

We analyzed the ^{12}CO J=3–2 spectra and noticed the spectra had wide wings. We suggest that there is an outflow in the S64 molecular cloud. Figure 2 shows three ^{12}CO J=3–2 lines as examples. According to Frerking & Langer (1982), if the wings are due to a rotating disk, a requisite central mass M_r (within a factor of 2) can be given by

$$M_r = \frac{V_r^2 r}{G} \ , \tag{1}$$

with V_r, r and G the rotating velocity, the radius of the hypothetical disk and the gravitational constant. Assuming the distance D of 700 pc given by Shaver & Goss (1970) and a V_r of 4.6 km s^{-1}, we obtain a radius of 0.8 pc and an M_r of 3940 $M_\odot$. This mass is much larger than the mass of the molecular cloud core of 100 or 260 $M_\odot$ estimated by Vallée et al. (1992) and 180 or 320 $M_\odot$ derived in this paper. Therefore, it is impossible that the wings are produced by a disk. We can also exclude the possibility that it is turbulence that produce the wings, because there is no neighboring source which can provide the huge energy supply to keep the turbulence over a long time.

The integral ranges we took are from –0.7 to 2.8 km s^{-1} for the blue wing, and from 5.7 to 8.4 km s^{-1} for the red wing. Figure 3 presents the integrated contour map of the outflow. It shows that the center of the outflow is located at the point (0, 0). We should add that we have taken a conservative upper limit for the integral of the red wing to avoid possible effects of other objects or a dirty background which are considered in the ^{12}CO J=1–0 spectra, and our observations have not covered the whole region of the blue lobe.

3.1.2 Outflow Parameters

The parameters of the outflow were estimated under the assumption of Local Thermal Equilibrium (LTE). We did not know the angle between the axis of the outflow and our line of sight, so following Goldsmith et al. (1984) a mean value of 45 degree was assumed.

The calculations of the physical parameters were all based on the theory of Radiative Transport in Molecular Lines (see Sun & Li 2003). The excitation temperature $T_{\rm ex}$ can be estimated from the CO lines. For the emission of molecular clouds, the central parts of the ^{12}CO lines are optically thick. Therefore we can estimate $T_{\rm ex}$ with the equations:

$$T_{\rm ex}(J=1-0)=\frac{5.53}{\ln[1+1/(T_a^*/5.53\eta_b+0.1545)]}\,, \tag{2}$$

and

$$T_{\rm ex}(J=3-2)=\frac{16.59}{\ln[1+1/(T_a^*/16.59\eta_b+0.0024)]}\,, \tag{3}$$

for the transitions of J=1–0 and J=3–2, respectively. In the above equations, a background temperature $T_{\rm bg}$=2.75 K was used, and T_a^* and η_b are the antenna temperature and the telescope beam efficiency, respectively. The largest intensities are 12.95 K for the ^{12}CO J=1–0 spectra and 16.48 K for ^{12}CO J=3–2. Using the two values, we obtain $T_{\rm ex}(J$=1–0)=34.4 K and $T_{\rm ex}(J$=3–2)=35.0 K, in good mutual agreement. We then adopted a general $T_{\rm ex}$ of 30 K for the entire cloud. The column density of CO can be estimated with the equation

$$N=\frac{3k}{8\pi^3B\mu^2}\frac{\exp[hBJ(J+1)/kT_{\rm ex}]}{J+1}\frac{T_{\rm ex}+hB/3k}{1-\exp[-2hB(J+1)/kT_{\rm ex}]}\int\tau{\rm d}\nu\,, \tag{4}$$

with B, μ and J the rotational constant, permanent dipole moment of the molecular and the rotational quantum number of the lower state in the transition, and T_r=T_a^*/η_b is the brightness temperature. On the other hand, from its definition, T_r can be expressed as

$$T_r=\frac{h\nu}{k}\Big[\frac{1}{\exp(h\nu/kT_{\rm ex})-1}-\frac{1}{\exp(h\nu/kT_{\rm bg})-1}\Big][1-\exp(-\tau)]\ . \tag{5}$$

Under the assumption that the wings are optically thin, $1-\exp(-\tau)\approx\tau$. For the transition of ^{12}CO J=3–2, introduction of Equation (5) into Equation (4) results in the column density:

$$N({\rm CO})_{\rm thin}=4.91\times10^{14}(T_{\rm ex}+0.92){\rm exp}\frac{33.18}{T_{\rm ex}}\int T_r{\rm d}\nu\ {\rm cm}^{-2}\ , \tag{6}$$

where $T_{\rm bg}$ is neglected.

However, studies have shown that even in the wings of lines, τ of ^{12}CO is often optically thick (e.g., Bally & Lada 1983; Snell et al. 1984; Choi et al. 1993; Wu et al. 2004), so some correction of the results is necessary. According to Garden et al. (1991), in the introduction of Equation (5) into Equation (4) we retain τ and then introduce a mean optical depth $\overline{\tau}$ as its approximation. Then, for ^{12}CO J=3–2, the column density is given by the equation

$$\begin{aligned}N({\rm CO})_{\rm thick}&=4.91\times10^{14}(T_{\rm ex}+0.92){\rm exp}\frac{33.18}{T_{\rm ex}}\int T_r\frac{\tau}{1-\exp(-\tau)}{\rm d}\nu\\&=4.91\times10^{14}(T_{\rm ex}+0.92){\rm exp}\frac{33.18}{T_{\rm ex}}\frac{\overline{\tau}}{1-\exp(-\overline{\tau})}\int T_r{\rm d}\nu\ .\end{aligned} \tag{7}$$

The precise value of $\overline{\tau}$ is difficult to calculate. Other researches (e.g. Bally & Lada 1983; Goldsmith et al. 1984; Shepherd & Churchwell 1996; Wu et al. 2004) showed that the optical depth of CO in molecular outflows is usually from about 1 to 8. So here we assume a $\overline{\tau}$ of 4 for a rough approximation.

A [^{12}CO]/[H_2] ratio of 10^{-4} is assumed in calculating the mass M. Also, we use a mean atomic weight of 1.36, as did Garden et al. (1991), on considering the mixture of hydrogen and helium. The momentum P and energy E of the outflow are respectively proportional to $\int T_r\nu{\rm d}\nu$ and $\int T_r\nu^2{\rm d}\nu$ and can be evaluated similarly to the mass. To define the lobes, a characteristic velocity, $V=P/M$, and a dynamic time scale $t_{\rm d}=R/V$, where R is the maximal size from the center to the edge of the lobe, are involved. The mechanical luminosity of the outflow and the driving force are estimated

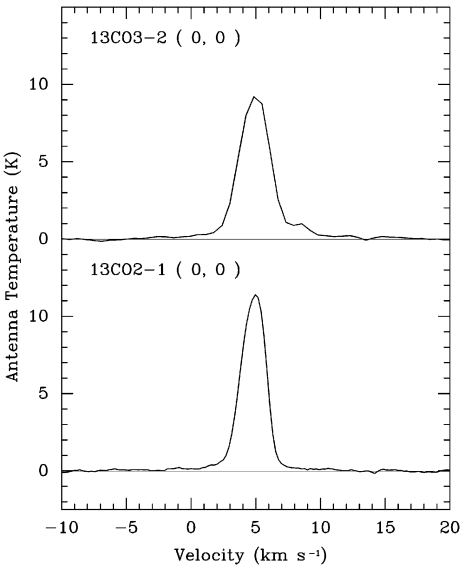

Fig. 4 ^{13}CO J=2–1 and ^{13}CO J=3–2 spectra of the (0, 0) point.

with $L = E/t_{\rm d}$ and $F = P/t_{\rm d}$. Further, by assuming the star wind velocity v=1000 km s^{-1} given by Lamers et al. (1995), the mass-loss rate of the central object is obtained from $\dot{M} = P/(t_{\rm d}v)$.

The results are listed in Table 1. Columns 2–5 present the outflow masses, momentum energies and maximal scales. Column 6 gives the outflow characteristic velocities. Columns 7–10 list in turn the time scale, driving force, mechanical luminosity and mass-loss rate.

Table 1 Parameters of the Outflow

Component		M	P	$E \times 10^{44}$	$R_{\rm max}$	V	$t_{\rm d}$	$F \times 10^{-5}$	$L \times 10^{-2}$	$\dot{M} \times 10^{-8}$
		[$M_\odot$]	[$M_\odot$ km s^{-1}]	[erg]	[pc]	[km s^{-1}]	[10^4yr]	[$M_\odot$ km s^{-1} yr^{-1}]	[$L_\odot$]	[$M_\odot$ yr^{-1}]
Red lobe	$\tau \ll 1$	0.51	2.42	0.86	0.58	4.72	12.0	2.03	0.59	2.03
	$\overline{\tau}$=4	2.10	9.90	3.51	0.58	4.72	12.0	8.28	2.39	8.28
Blue lobe	$\tau \ll 1$	0.48	2.50	1.03	0.35	5.22	6.62	3.78	1.27	3.78
	$\overline{\tau}$=4	1.95	10.2	4.20	0.35	5.22	6.62	15.4	5.16	15.4
Total	$\tau \ll 1$	0.99	4.92	1.89	—	—	—	5.81	1.86	5.81
	$\overline{\tau}$=4	4.05	20.8	7.71	—	—	—	23.7	7.55	23.7

The outflow is rather weak, with a corrected total mass of only 4.05 $M_\odot$ (2.10 $M_\odot$ for the red and 1.95 $M_\odot$ for for the blue lobe), assuming a mean optical depth of 4. That the value of $\overline{\tau}$ may be underestimated is indicated by the faint infrared emission, and we may have neglected the mass of the cold regions which lack ^{12}CO J=3–2 emission. In addition, the mass of the red lobe should be underestimated due to the conservative integral range, and for the blue lobe, we only estimated the mass of the observed region.

3.2 Core

3.2.1 Isotopic Cores

The observations of ^{13}CO J=2–1 and ^{13}CO J=3–2 lines are used to define the core of the molecular cloud. Figure 4 shows the ^{13}CO J=2–1 and ^{13}CO J=3–2 spectra at position (0, 0).

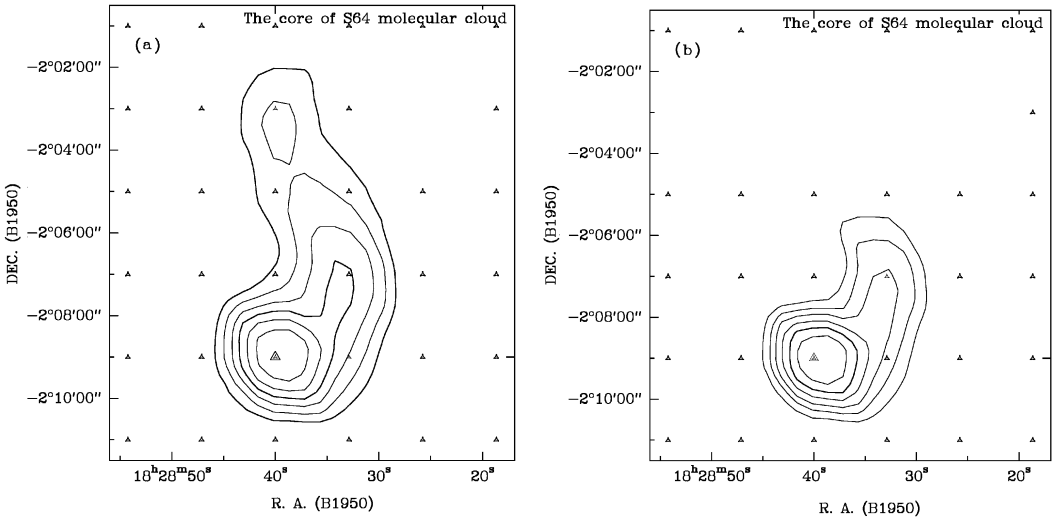

Fig. 5 Integrated maps of the core (a) from the ^{13}CO J=2–1 lines; (b) from the ^{13}CO J=3–2 lines. The contour levels are from 40%–90% at intervals of 10%.

For both spectra, we take an integral range of the core from 3.4–6.3 km s^{-1}. Then we obtain the contour maps presented in Figure 5. The centers of the cores in the two maps are well coincident with each other, and the ^{13}CO J=3–2 core seems to be more compact than its isotopic counterpart. It is natural that the excitation of the higher energy level of ^{13}CO needs a greater density and temperature, so the ^{13}CO J=3–2 core is closer to the centre than is the ^{13}CO J=2–1 core. The positions of the two cores are also coincident with the ^{13}CO J=1–0 result of Vallée et al. (1992).

3.2.2 Core Parameters

The physical parameters of the core are estimated with the ^{13}CO data. Since at a high density, the core is not always optically thin even for ^{13}CO. Assuming that the cloud is in LTE, the optical depth τ can be estimated with the two equations:

$$\tau(^{13}\mathrm{CO}2-1) = -\ln\Big[1 - \frac{Tb_r/10.58}{1/(\exp\frac{10.58}{T_{\rm ex}} - 1) - 0.022}\Big], \tag{8}$$

and

$$\tau(^{13}\mathrm{CO}3-2) = -\ln\Big[1 - \frac{T_r/15.87}{1/(\exp\frac{15.87}{T_{\rm ex}} - 1) - 0.003}\Big], \tag{9}$$

where a background temperature of 2.75 K was used. Two values of τ are acquired: 1.01 with the ^{13}CO J=2–1 spectrum, and 0.81 with ^{13}CO J=3–2 spectrum. Therefore, the column density of ^{13}CO should be given by:

$$N(^{13}\mathrm{CO}) = \frac{3k(T_{\rm ex} + hB/3k)}{8\pi^3\mu^2B(J+1)}\exp\frac{hBJ(J+1)}{kT_{\rm ex}}\Big[1 - \exp\frac{-2hB(J+1)}{kT_{\rm ex}}\Big]^{-1}\int \tau \mathrm{d}\nu\,. \tag{10}$$

Further, assuming a [^{13}CO]/[H_2] ratio of 1.12×10^{-6}, we can evaluate the density and the mass. Here a mean atomic weight of 1.36 is again used. In the calculations we define the core by the 50% contour of the integrated intensity. The results are listed in Table 2. Columns 2–5 present the optical depth, the core mass, and the column densities of ^{13}CO and H_2. Column 6 gives the mean

Table 2 Parameters of the Core

Transition	τ	M $[M_\odot]$	$N(^{13}\mathrm{CO})$ $[10^{16}\ \mathrm{cm}^{-2}]$	$N(\mathrm{H_2})$ $[10^{22}\ \mathrm{cm}^{-2}]$	R_{mean} [pc]	$n(\mathrm{H_2})$ $[10^{3}\ \mathrm{cm}^{-3}]$
^{13}CO J=2–1	1.01	319	1.97	1.76	0.83	6.85
^{13}CO J=3–2	0.81	188	1.45	1.30	0.68	6.18

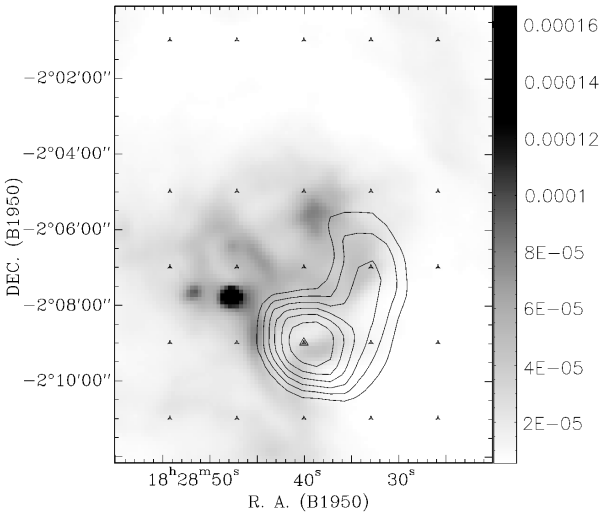

Fig. 6 A comparison of ^{13}CO J=3–2 core and MSX 8 μm emission. The ^{13}CO J=3–2 contour levels are from 40%–90% at intervals of 10%. The background is the MSX 8 μm map, and the unit of its color key is W m^{-2} sr^{-1}.

size of the long and short axes, and Column 7, the density of H_2 calculated basing on the mean size.

The derived mass is 319 $M_\odot$ from the ^{13}CO J=3–2 transition, and 188 $M_\odot$ from the J=2–1 transition. The difference of the two results is mostly due to the smaller region of the ^{13}CO J=3–2 core. The transition of ^{13}CO J=3–2 needs higher density and temperature, so we have neglected the mass of the colder and sparser outer region in the calculation. Both of our results are larger than the ^{13}CO J=1–0 result of 100 $M_\odot$ given by Vallée et al. (1992), where the mass was estimated with a radius of 0.4 pc, a larger $[^{13}\mathrm{CO}]/[\mathrm{H_2}]$ ratio of 2×10^{-6} and a shorter distance of 600 pc.

4 DISCUSSION AND CONCLUSIONS

An HII region is a tracer of a formation region of massive stars. Several studies have been made on the HII region S64 and its cold molecular cloud. Zeilik & Lada (1978) advanced a blister model where the S64 HII region was expanding away from the surface of the molecular cloud. It means that at least one massive star had been formed in the molecular cloud. In this paper we have identified a weak outflow, which indicates that star formation is going on. Though the mass result has been corrected, it may be underestimated for several reasons (see Sect. 3.1.2). We can not determine the collimation of the outflow because the limited coverage of the observed region. As shown in Figures 3, 4 and 5, the center of the outflow coincides with the position of the core, as well as the CO peak of molecular cloud given by Zeilik & Lada (1978). Therefore, we suggest that the driving source of the outflow is in the core.

We compared our CO contour maps with the infrared data of MSX and IRAS, and found that the core deviates from the regions of strong infrared emission. The departure suggests that the source is deeply embedded in the molecular cloud. Figure 6 shows that the core contours of ^{13}CO J=3–2 overlapped on the MSX 8 μm map. However, we noticed some rather weak 8 μm emission in the core region, and that there were several MSX point sources near the center of the core. That may indicate some early star formation activities deep inside the core. Depending on the transition used, the mass of the core we calculated is either 188 or 319 $M_{\odot}$, which is sufficient for the formation of a massive star. Observations with higher resolution are needed to make clear the correlation between the millimeter and infrared emission, and we hope that the observations with other molecular like HCO^+ or H_2N^+ can reveal the internal structures of the core.

We suggest that the expansion of the HII region disturbed the ambient molecular gas, stimulating the formation of other stars. There may be one or more forming stars in the core, and the outflow should belong to one of them. We do not know the structure of the core and whether one of the MSX point sources is the counterpart of the core. However, we can say that the driving source of the outflow is rather young, because its emission in mid-infrared wavelengths is faint or non-existent. For further study, more observations with higher resolution and larger area are needed.

Acknowledgements We are grateful to Martin Miller for the kind help during the observation. We would like to thank Binggang Ju and other staff of Qinghai Station, PMO, for their significant assistance in the observation. The project is supported by Grants 10133020, 10128306 and 10203003 of National Natural Science Foundation of China (NSFC), and G1999075405 of NKBRSF.

References

Bally J., Lada C. J., 1984, ApJ, 265, 824
Choi M., Evans N. J., II, Jaffe D. T., 1993, ApJ, 417, 264
Crutcher R. M., Chu Y. H., 1982, In: R. S. Roger, P. E. Dewdney, eds., Regions of Recent Star Formation, Reidel, Dordrecht, Holland: Ap&SS Lib., 93, p.53
Esimbek J., Wu Y. F., Wang J. Z., 2005, ChJAA, 5, 587
Frerking M. A., Langer W. D., 1982, ApJ, 256, 523
Garden R. P., Hayashi M., Gatley I. et al., 1991, ApJ, 374, 540
Goldreich P., Kwan J., 1974, ApJ, 189, 441
Goldsmith P. F., Snell R. L., Hemeon-Heyer M., 1984, ApJ, 286, 599
Lamers Henny J. G. L. M., Snow, Theodore P., Lindholm Douglas M., 1995, ApJ, 455, 269
Sharpless S., 1959, ApJS, 4, 257
Shaver P. A., Goss W. M., 1970, Aust. J. Phys. Astrophys. Suppl., 14, 133
Shepherd D. S., Churchwell E., 1996, ApJ, 457, 267
Snell R. L., Scoville N. Z., Sanders D. B., Erickson N, R., 1984, ApJ, 284, 176
Sun J., Li S. Z., 2003, Introduction of Molecular Astrophysics, Beijing normal university press, Beijing
Vallée J. P., 1987, A&A, 178, 237
Vallée J. P., MacLeod J. M., 1991, A&A, 250, 143
Vallée J. P., MacLeod J. M., 1994, AJ, 108, 998
Vallée J. P., Guilloteau S., MacLeod J. M., 1992, A&A, 266, 520
Westerhout G., 1958, Bull. Astron. Inst. Netherlands, 14, 215
Wood D. O. S., Churchwell E., 1989, ApJS, 69, 831
Wu J. W., Wu Y. F., Wang J. Z. et al., 2002, ChJAA, 2, 33
Wu Y. F., Wei Y., Zhao M. et al., 2004, A&A, 426, 503
Yorke H. W., Tenorio-Taglio G., Bodenheimer P., 1983, A&A, 127, 313
Zeilik M., Lada C. J., 1978, ApJ, 222, 896